Nuclear Instruments and Methods in Physics Research B 319 (2014) 171–176

Contents lists available at ScienceDirect

Nuclear Instruments and Methods in Physics Research B

journal homepage: www.elsevier.com/locate/nimb

# Structural and elemental X-ray microanalysis with synchrotron radiation in confocal geometry

Carlos M. Sosa [a], H. Jorge Sánchez [a,c], Carlos A. Pérez [b], Roberto D. Perez [a,c,*]

[a] IFEG-CONICET, (X5016LAE) Ciudad Universitaria, Córdoba, Argentina
[b] Laboratório Nacional de Luz Síncrotron – LNLS, POB 6192, 13084-971 Campinas, SP, Brazil
[c] FAMAF, Universidad Nacional de Córdoba, (X5016LAE) Ciudad Universitaria, Córdoba, Argentina

ARTICLE INFO

*Article history:*
Received 26 June 2013
Received in revised form 27 September 2013
Available online 13 November 2013

*Keywords:*
3D X-ray microanalysis
Polycapillary optics
EDXRF
EDXRD

ABSTRACT

A spectrometer for 3D structural and multielemental X-ray microanalysis with synchrotron radiation is presented in this work. It is based on the combination of the energy dispersive X-ray fluorescence and diffraction with polycapillary optics. The 3D spatial resolution was achieved by the superposition of the foci of two lenses arranged in confocal geometry. The parameters that affect the performance of the spectrometer were study in detail giving rise to a simplified calibration method for depth profile analysis. Two specific examples were included to illustrate the use of the spectrometer in order to identify their possible application fields.



## 1. Introduction

A recent development in X-ray microanalysis is the expansion of spatial resolution into the depth with the help of a confocal setup using X-ray optics. The foci of two lenses, one in the excitation channel and other in the detection channel, define a micro-volume for probing the sample. Fluorescence and scattered radiation, ideally, are detected only from this volume. During the last years, experiments with confocally aligned X-ray lenses have been performed at various laboratories around the world [1–5]. This setup proved to be capable to supply three-dimensional or depth-sensitive information on the elemental composition of a sample with a minimum spatial resolution of 10 μm. The usefulness of the new 3D micro-XRF method has already been shown at several applications [1–5].

The confocal setup implemented with polycapillary optics and polychromatic sources allows expanding its applications not only for elemental analysis but also for structural analysis. Effectively, the X-ray scattering produced by a continuous excitation spectrum in the probing volume can be used to obtain a diffraction pattern of the sample by means of Micro X-ray Diffraction Analysis (micro-XRD) in the Energy Dispersive (ED) configuration [6,7]. The continuous spectrum of the polychromatic source creates Laue diffraction peaks that originate from different crystallographic planes according to Bragg's condition. Then, the X-ray optics in the detection channel has to collect X-rays photons with a wide energy range. Polycapillary lenses are the ideal candidate to successfully satisfy this requirement, since they allow a broad energy bandpass.

In the energy dispersive X-ray diffraction the dispersion angle is fixed and the detected energy is scanning through the range source. It can be electronically done by an energy dispersive X-ray detector. Thus, it is possible to implement simultaneously the 3D micro-XRD and the 3D micro-XRF without the inclusion of any other additional component as an expensive goniometer or monochromator. It is a modern concept in X-ray spectrometry developed in the last few years which could be very useful for elemental and structural analysis with spatial resolution [8].

In this work confocal three-dimensional energy-dispersive micro XRD and micro-XRF was implemented using polycapillary optic. We used half lenses manufactured in our laboratory which were characterized using an experimental process described in a previous paper [9]. The lenses have low divergence in the order of milliradians allowing obtaining a good angular resolution and can efficiently focus the synchrotron beam. A characterization of the spectrometer which includes the determination of the sensitivity of the confocal setup and the lattice spatial resolution of the diffractometer is presented in this work.

## 2. Materials and methods

The experiment was carried out in the D09B-XRF beamline of the Brazilian Synchrotron Light Source (LNLS) using white beam. A silicon drift X-ray detector with 150 eV of resolution at 5.9 keV

* Corresponding author at: IFEG-CONICET, (X5016LAE) Ciudad Universitaria, Córdoba, Argentina.
*E-mail address:* danperez@famaf.unc.edu.ar (R.D. Perez).

0168-583X/$ - see front matter © 2013 Elsevier B.V. All rights reserved.
http://dx.doi.org/10.1016/j.nimb.2013.10.021

was positioned at 44° to the photon beam on the horizontal plane. This system was mounted on a motorized XYZ stage with manual goniometers to tilt the detector. Suspended from the snout of the silicon drift detector, a fixed holder holds a half monolythic polycapillary with its optical axes centered and normal to the window of the detector. In the excitation channel a similar glass polycapillary was mounted in a special motorized gimbal. Both lenses had a focal distance of 20 mm with a focal dimension of 75 μm, a divergence of 2 mrad and a transmission efficiency of 20% for the mean energy of the excitation spectrum [9]. Samples were mounted vertically at 22° of the incident direction on a motorized XYZ sample stage with spatial resolution of 0.6 μm. Aligned ionising chambers at the entrance of the first polycapillary and behind the sample holder were used to align efficiently the excitation channel. In addition, a CCD camera was placed behind the sample holder to determine the position of the incident beam. A digital optical microscope focused on the sample was employed to distinguish details on the area excited by the incident beam. The experimental arrangement with the relevant geometrical parameters is shown in Fig. 1.

Once the polycapillary of the excitation channel was aligned, we oriented the axis of the polycapillary of the detection channel at 44° from the incident direction on the horizontal plane. Then, a silicon wafer (111) was placed in the sample holder. Using the motorized XYZ stage on the detector holder, we positioned the end of the polycapillary at 20 mm from the excitation point of the sample. Once a preliminary alignment of the setup was found, several linear scans of the probing volume through the normal direction of the foil were performed to improve the position of the polycapillary of the detection channel. For all scans, the counting live-time for each point was 10 s/step and the step size was 10 μm. The maximum of the diffraction peaks were recorded for each linear scan. They were considered as a test parameters of the quality alignment of the polycapillary. The greatest value registered for these intensities corresponds to the optimal alignment of the polycapillary. In this way the incident and emergent angles could be defined with high precision.

To determine the sensitivity of the spectrometer, we performed linear scans through the normal direction of pure foils. We used standard ultra thin foils (Micromatter) of Ti, V, Fe, Cu. ZnTe and Au with high purity (99.9%) and thickness in the order of the micrometer. For all scans, the counting live-time for each point was 40 s/step and the step size was 10 μm. As a final result, scanning curves of the XRF intensity versus depth were obtained for each element present in the set of thin films. To determine the detection limit for elemental analysis, we measured two biological tissues prepared as presses pellets. One of the samples was the reference material NIST 1577c of dried bovine liver and the second

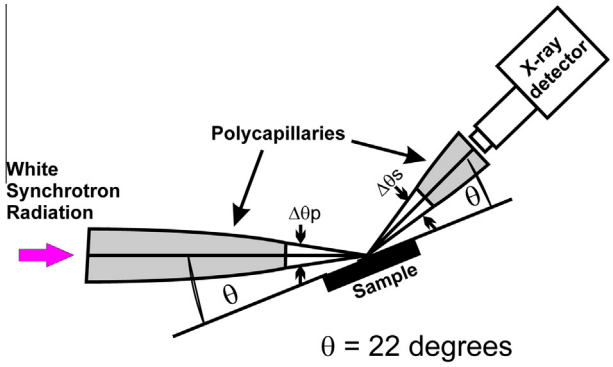


**Fig. 1.** Experimental setup of the spectrometer. The contribution to the angular resolution of the divergence of both lenses is shown.

was a dried rat liver analyzed in a previous work [10]. They were scanned in depth with a counting live-time for each point of 60 s/step and a step size of 10 μm.

## 3. Theory

### 3.1. Confocal micro-XRF

Assuming a homogeneous film of thickness $D$, the intensity of a specific X-ray fluorescence line of an element $i$ excited by a polychromatic source as a function of the normal coordinate $x$ can be written as [11]:

$$Ip_i(x) = \int_0^{E_m} \rho_i I_0(E)\,\tau_{F,i}(E) \left( \int_0^D \eta_i(E, x' - x)\, \exp(-\tilde{\mu}_i(E)\,x')\,dx' \right) dE \tag{1}$$

where $E_m$ is the maximum energy of the incoming photons, $I_0(E)$ is the incoming photon flux of energy $E$, $\rho_i$ is the density (in g/cm$^3$) of the $i$-element in the sample, $\tau_{F,i}$ is the production cross section (in cm$^2$/g) for the measured X-ray line of the $i$-element at energy $E$, $\eta_i(E,x)$ is the sensitivity profile of the spectrometer for the $i$-element at position $x$, and $\tilde{\mu}_i$ is the effective linear mass attenuation coefficient at energy $E$ for the $i$-element defined as follows:

$$\tilde{\mu}_i = \sum_{j=1}^{r} \rho_j \left( \frac{\mu_j(E)}{\sin(\theta_0)} + \frac{\mu_j(E_i)}{\sin(\theta_1)} \right) \tag{2}$$

where $\rho_j$ is the density of the $j$-element, $\mu_j(E)$ is the mass attenuation coefficient of the $j$-element at energy $E$, $E_i$ is the energy of the X-ray line of the $i$-element, $\theta_0$ and $\theta_1$ are the medium angle of the impinging beam and detected beam respectively.

The formula shown in Eq. (1) is the key for the quantitative multielemental analysis by fundamental parameters method. Besides of the input of emission and absorption probabilities, the calculations require the precise knowledge of the sensitivity profile of the spectrometer.

### 3.2. Confocal micro-XRD

The confocal micro-XRD combines the Energy Dispersive X-ray Diffractometry (EDXRD) with the 3D spatial resolution of the confocal setup. EDXRD is a well known method which can be implemented without complex mechanical motions of the detector or source since the diffraction angle is fixed. It takes advantage of the semiconductor X-ray detectors technology to electronically scan the scattered intensity for energy, looking for Laue diffraction peaks. These peaks originate from constructive interference in the different crystallographic planes according to Bragg's condition:

$$d = \frac{6.199}{E \sin\theta} \tag{3}$$

where $d$ is the interplanar spacing of the lattice planes in Ångstroms, $2\theta$ is the diffraction angle and $E$ is the scattered energy in keV. The full with at half maximum of a diffraction peak $\Delta E_{FWHM}$ can be taken as the minimum energy separation between two resolved diffraction peaks. Considering that the diffraction angle at the maximum of the diffraction peaks is $\theta$, then, the lattice spacing resolution of the spectrometer is related with $\Delta E_{FWHM}$ by means of the following Eq. (12):

$$\Delta d = -\frac{6.199}{E \sin\theta} \Delta E_{FWHM} \tag{4}$$

Evaluating the width of different diffraction peaks of a monocrystalline sample, it is possible to obtain directly the lattice spacing resolution of the spectrometer for different energies. Fur-

thermore, it can be related with the precision of $E$ and $\theta$ by means of statistical error propagation defined by the Bragg equation:

$$\left(\frac{\Delta d}{d}\right)^2 = (\Delta\theta\ ctg\,\theta)^2 + \left(\frac{\Delta E_D}{E}\right)^2. \quad (5)$$

The first term in the right hand side of this equation corresponds to the widening of the diffraction peaks due to angular divergence of the diffractometer, which depends on the polycapillary lenses in the excitation and detection channel. Since the size of the confocal volume is a function of energy, it follows that the term $\Delta\theta$ also depends on $E$. The second term in the previous equation represents the inherent resolution of the detection system which is given by [12]:

$$\left(\frac{\Delta E_D}{E}\right)^2 = \frac{\left(\Delta E_{amp}\right)^2 + \left(2.355(F\varepsilon E)^{\frac{1}{2}}\right)^2}{E^2} \quad (6)$$

where $\Delta E_{amp}$ is due to noise in the solid state detector and preamplifier, $F$ is the Fano factor and $\varepsilon$ is the energy necessary to create an electron–hole pair. Combining the last three equations it is possible to deduce the energy dependence for the relative resolution of the diffractometer:

$$\frac{\Delta d}{d} = \frac{\sqrt{A_1 + A_2E + E^2(A_3 + A_4E + A_5E^2)^2}}{E} \quad (7)$$

where $A_i$ are constants. For $\Delta\theta$ a second order polynomial dependence with energy was assumed according to the experimental results observed in our own measurements as well as for other authors [7,13]. The fitting of Eq. (7) to the relative lattice spacing resolution calculated for a monocrystalline sample by Eq. (4) allows obtaining the calibration of the diffractometer.

### 3.3. Sensitivity of the confocal setup

The sensitivity profile is the theoretical description of the probing volume of the confocal setup. For depth profile analysis it can be written as [11]:

$$\eta_i(E,x) = A_i(E)\ \exp(-x^2/2\,\sigma_i(E)^2), \quad (8)$$

where:

$$A_i(E) = \frac{\Omega\,\varepsilon(E_i)\,\sigma_D^2(E_i)T_A(E)\,T_D(E_i)}{2\pi\sigma_i^2(E)}$$

$$\sigma_i^2(E) = \left(\frac{\sigma_A(E)}{2}\right)^2 + \left(\frac{\sigma_D(E_i)}{2}\right)^2$$

$\Omega$ is the solid angle accepted by the lens in the detection channel, $\varepsilon$ is the detector efficiency, $T_A$ and $T_D$ are the transmission of the lenses in the excitation and detection channel respectively, and $\sigma_A$ and $\sigma_D$ are the focal sizes of the lenses in the excitation and detection channel respectively. $\eta_i(E,x)$ is a dimensionless profile that multiplied by $\tau_{F,i}(E)$ and $\rho_i$ gives the probability of XRF emission of element $i$ from a thin film of the sample placed at $x$ position. $A_i(E)$ is the maximum value of the sensitivity profile at energy $E$ and $\sigma_i(E)$ is the size of the confocal volume projection in the normal direction of the sample. In particular, for a very thin film of thickness $d$ we have that the X-ray fluorescence intensity of $i$ element is given by:

$$Ip_i(x) = \int_0^{E_m} \rho_i I_0(E)\,\tau_{F,i}(E)\,\eta_i(E,x)\,d \quad (9)$$

Thus, through a vertical scan of a thin film reference standard sample of knowledge thickness and composition, it is possible to determine the sensitivity of the spectrometer for depth profile analysis. The use of a set of thin films increases the accuracy of the determination.

## 4. Results and discussion

Fig. 2 shows the energy dependence of the sensitivity parameters $A_i(E)$ and $\sigma_i(E)$ of titanium for the confocal setup implemented in the XRF beamline of the LNLS. The sensitivities were obtained by an iterative process where Eq. (9) is fit on the experimental XRF intensity-depth profiles. The fits are based on a simplified process employing piecewise linear functions for $T_A(E)$ and $\sigma_A^2(E)$ whose breakpoints are the absorption edges of the elemental components present in the set of thin films. As first approximation the foci of both lenses were assumed equal, since both of them have been manufactured by the same process. The order of the elements in the iterative process is defined by the value of their absorption edges which is chosen as gradually decreasing in each step. For the scanning curve of the $i$-element, the method fits the sensitivity function of $i$ in the partition between absorption edges of the elements $i$ and $(i+1)$. The contribution on the XRF intensity coming from the partitions of higher energies is evaluated using the sensitivity calculated with the parameters $T_A(E)$ and $\sigma_A^2$ obtained in previous fits. In this way the information extracted from each scan is used to overcome instabilities in the fitting process on the remainder scans.

The size of the confocal volume $\sigma_i(E)$ is a decreasing function of incident energy. It is a consequence of the lower divergence of the X-ray lenses at higher energies caused by smaller values of the total reflection angle of glass. The proportional factor $A_i(E)$ of the sensitivity shows a wide asymmetric maximum as a function of incident energy with a strong decrease for lower energies and a soft decrease for higher energies. The behavior is similar to the transmission function of half polycapillaries showing that the main contribution to $A_i(E)$ comes from the transmission properties of the focusing optics.

The resolution of the lattice spacing was obtained from the diffraction spectrum of a single-crystal of Si(1 1 1). It consisted of four diffraction peaks produced by the first orders of Bragg reflections on the atomic planes (1 1 1) of Si. The rate between the FWHM and the center of each peak was taken as a direct calculation of the relative resolution of the diffractometer (see Fig. 3). Both

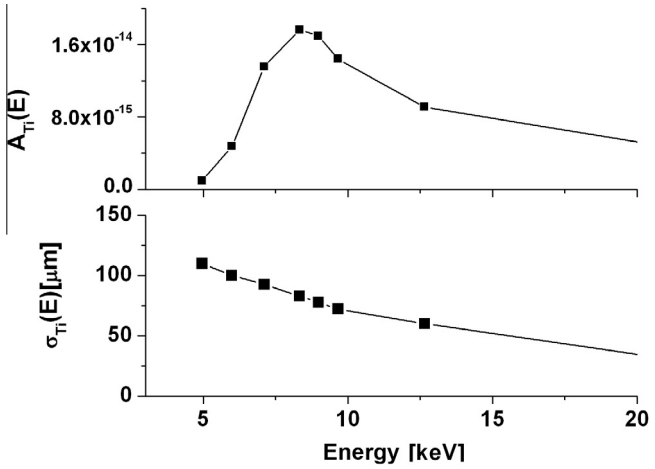


**Fig. 2.** Parameters of the sensitivity profile for titanium as a function of the incident energy. The first curve is the maximum $A_i(E)$ of the sensitivity profile and the second curve is the size of the probing volume.

parameters were obtained by fitting a Gaussian function at each diffraction peak. The experimental ordered pairs $(\Delta d/d;E)_i$ were fitted with Eq. (7) to obtain the calibration of the diffractometer at the energy interval of the X-ray source. The relative resolution showed an almost linear decrease with incident energy ranging in the interval [1%; 2%]. The main contribution comes from the energy resolution of the detector, as can be seen in the comparison of Fig. 3. The characteristics of the detector were determined by technicians of the LNLS beamline by measurements of pure standards. Furthermore, the angular resolution of the diffractometer can be calculated from Eq. (4). It showed a decrease with incident energy which agree with the reduction of the divergence of the polycapillary optics previously discuss and reported by other authors [7,13].

As an example of the applicability of the spectrometer, the following three different species of Cu were analyzed: metal Cu, CuO and $Cu_2O$. The copper oxides were prepared as pressed pellet, while metal Cu was a standard pure foil (Alfa Aesar). Fig. 4 shows the spectrum for each species with the diffraction and the XRF peaks. For all spectra the acquisition time was 150 s. While the XRF peaks are almost equal in the three spectra, the diffraction peaks show a strong dependence with the species of copper. For each species the diffraction peaks were identified by means of a diffraction database. The prominent differences between the diffraction and XRF peaks are caused by two effects. First, the XRF peaks receive contributions from the whole excitation spectrum with energies higher than the absorption edge of Cu, while the diffractions peaks only receives contribution of the coherent scattering of incident photons of a well defined energy. Second, the photoelectric effect has a probability one order of magnitude higher than coherent scattering in the energy range of our X-ray source. Both effects can be minimized scanning the incident energy with a monochromator but increasing the acquisition time.

The possibility of depth profiling analysis was tested with an artificial sample of two layers: a thin deposit of $CO_3Ca$ over a thin foil of mica. A linear scan through the normal direction of this sample was done. The counting live-time for each point was 60 s/step and the step size was 25 μm. Fig. 5 shows the variation in depth for some diffraction peaks of mica and calcite, the Kα-XRF lines of Ca and Fe. As was expected, the diffraction peak of mica and XRF line of Fe have appreciated intensity at positions into the foil of mica, while the diffraction peaks of calcite and XRF line of Ca have appreciated intensities at positions into the layer of calcite.

The detection limit for the elemental microanalysis of biological tissues is shown in Table 1. The maximum XRF intensities in the depth scan of the standards were employed to calculate the detection limit. It has a minimum for Cu in agreement with the energy dependence of the sensitivity profile obtained previously. It is interesting to highlight that the calculation of the detection limit by means of the approximation of Eq. (1) for low concentrations is expressed in [g/cm$^3$]. However the Table 1 includes the detection limits as weight fractions in order to compare with traditional values. An estimation of the detection limit for structural microanalysis is possible to obtain assuming a linear dependence of the XRD intensity with the volumetric density of the material phase. It is a good approximation in our spectrometer because the XRD peaks are comparable to the background signal. Then it is possible

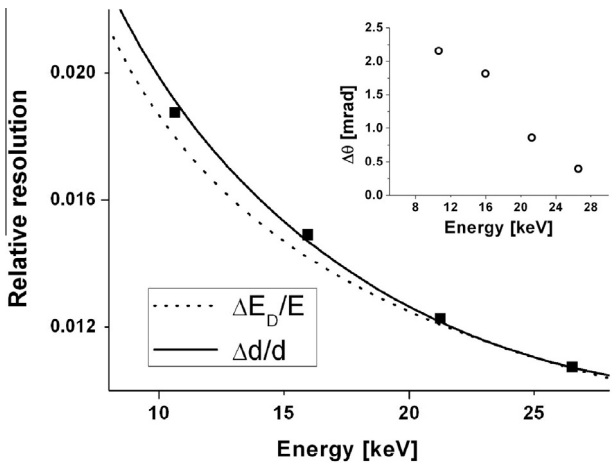


**Fig. 3.** Lattice spacing resolution of the spectrometer versus incident energy compare to the energy resolution of the detection system. The insert shows the angular divergence of the confocal setup calculated by Eq. (4).

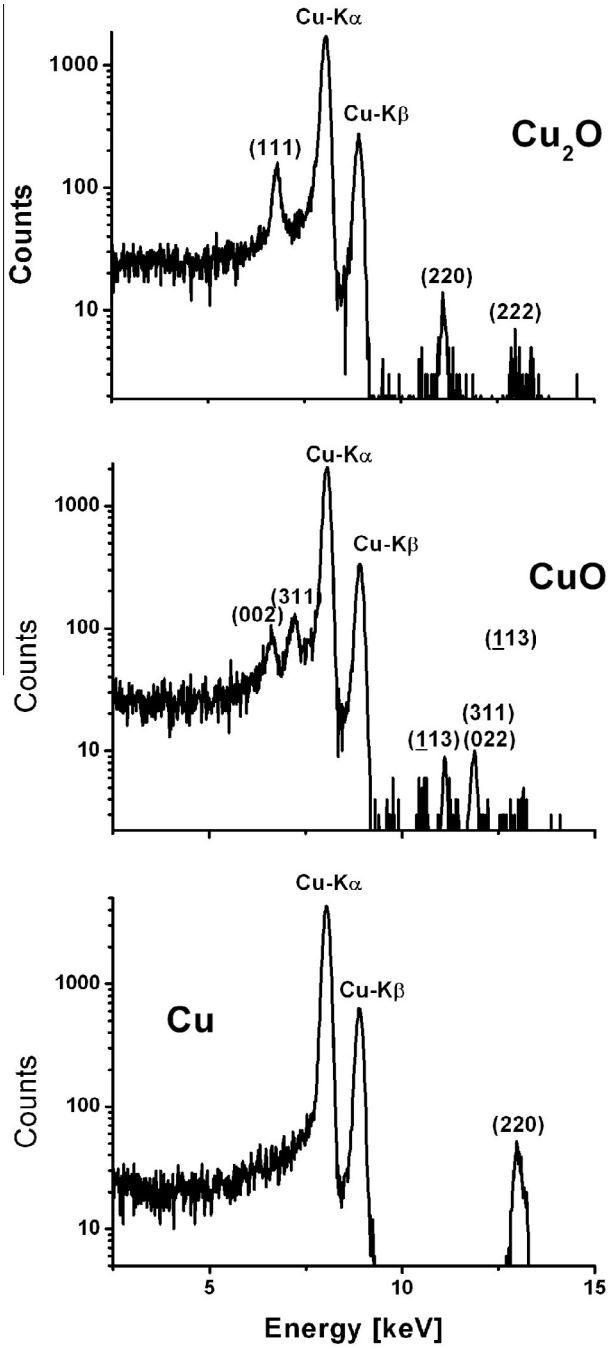


**Fig. 4.** Spectra for three different species of copper with an acquisition time of 150 s showing X-ray fluorescence and diffraction peaks.

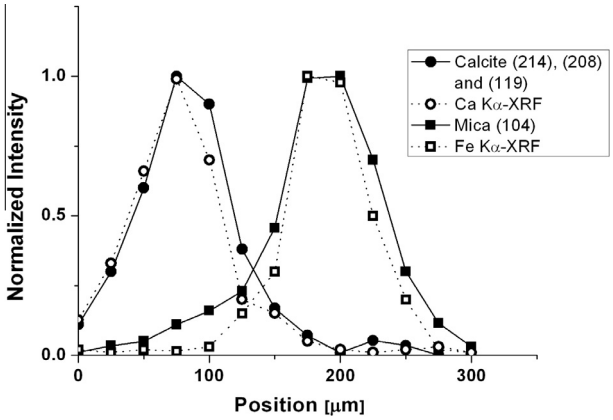


**Fig. 5.** Depth profile analysis of X-ray fluorescence and diffraction peaks of an artificial sample made of a calcite layer on mica substrate. For each scan the intensities were normalized with respect to the maximum of the profile. The acquisition time for each point in the scan was 60 s.

**Table 1**
Detection limit for some element calculated for dried biological tissue prepared as pressed pellet. The first line corresponds to weight fractions in ppm and the second line is for volumetric densities in g/cm$^3$.

| | K | Ti | Mn | Fe | Ni | Cu | Zn | As |
|---|---|---|---|---|---|---|---|---|
| LD[ppm w/w] | 2300 | 262 | 156 | 108 | 41 | 30 | 35 | 150 |
| LD [μg/cm$^3$] | 2800 | 310 | 190 | 130 | 49 | 36 | 42 | 180 |

to relate the registered XRD intensity with the detection limit by the formula:

$$DL = \frac{3\rho_\alpha\sqrt{N_{\mathrm{Bkg}}}}{N_{\mathrm{XRD}}}$$

where $\rho_\alpha$ is the volumetric density of the phase α, $N_{\mathrm{XRD}}$ is the number of counts in the XRD peak and $N_{\mathrm{Bkg}}$ is the number of counts in the background of the XRD peak. Thus the detection limit of the $Cu_2O$ phase in a Cu matrix is 0.30 g/cm$^3$ (5% w/w) with 150 s of acquisition time. In this calculation we used the higher diffraction peak obtained at the position of higher scattering in the depth scan. For mica in a matrix of silicate rock we obtained a detection limit of 0.12 g/cm$^3$ (4.3% w/w). It is important to highlight that the presented values are useful to illustrate the behavior of the spectrometer but they are not for a general use since the detection limit depends on the sample matrix.

The results obtained in the simplified calibration procedure show that the structural microanalysis with the proposed spectrometer has limitations in resolution and detection limit. These limitations can be successfully minimized by modern arrangements with X-ray area detectors in Angular Dispersive (AD) configuration [14,15]. In this case the acquisition times are similar than ED configuration but with more reliable peaks intensities and better momentum resolution. However, the energy resolution of these detectors still is not as good as the energy dispersive semiconductor detectors even for the most advanced devices [14]. Thus, a combined spectrometer for micro XRF/XRD in AD configuration improves micro-XRD analysis but declines micro-XRF performance. Since the opposite is valid for the ED configuration with semiconductor detectors, it is clear that the setup proposed in this paper is recommended for those studies where micro-XRF analysis is of priority interest and/or micro-XRD analysis not demand high momentum resolution or low detection limits. Favorable conditions for the spectrometer are founded, for example, in archeometry or analysis of amorphous materials. In archeometry paintings usually have a stratified structure with layers made of phases at high concentrations as $CO_3Ca$, $SO_3Ca$, PbO or amorphous materials as canvas or woods [8]. The study of amorphous materials by EDXRD, treated extensively in the literature [12], is characterized by low requirements on sensitivity and lattice resolution. We are particularly interested in apply our spectrometer to study biological tissues where elemental distribution and phase identification are viable by the spectrometer [16].

## 5. Conclusions

In this work a combined spectrometer for elemental and structural 3D microanalysis with synchrotron radiation is presented. To calibrate the spectrometer a simplified method has been developed which gives the sensitivity of the confocal setup and the lattice spacing resolution for structural studies. The higher sensitivity was obtained for incident energies with simultaneously greater values for the X-ray transmission of both lenses. In our experimental setup it happens for photons with energies ranging in the interval [5 keV; 10 keV]. For structural analysis it should contain the diffraction peaks under study by means of a convenient selection of the reflection angle with the Bragg equation.

The performance of the spectrometer was illustrated with the analysis of two specific artificial samples. They showed that the setup successfully combines the spatial resolution with short acquisition times for elemental and structural microanalysis. The main limitation of the spectrometer lies in the high detection limit and modest resolution for structural microanalysis. Taking this in consideration it is possible to identify possible application fields of the spectrometer as archeometry or amorphous materials studies.

## Acknowledgments

This work was partially supported by the Brazilian Synchrotron Light Source (Under Scientific Project LNLS D09B-XRF-4229) and CONICET from Argentina. We are also grateful to the LNLS team for perfect running conditions.

## References

[1] E. Bulska, I.A. Wysocka, M.H. Wierzbicka, K. Proost, K. Janssens, G. Falkenberg, In vivo investigation of the distribution and the local speciation of Selenium in *Allium cepa* L. by means of microscopic X-ray absorption near-edge structure spectroscopy and confocal microscopic X-ray fluorescence analysis, Anal. Chem. 78 (2006) 7616–7624.
[2] B. Kanngießer, W. Malzer, I. Reiche, A new 3D micro X-ray fluorescence analysis setup-first archaeometric applications, Nucl. Instr. Meth. Phys. Res. B211 (2003) 259–264.
[3] B. Vekemans, L. Vincze, F.E. Brenker, F. Adams, Processing of three-dimensional microscopic X-ray fluorescence data, J. Anal. At. Spectrom. 19 (2004) 1302–1308.
[4] S. Tianxi et al., Characterization of a confocal three-dimensional micro X-ray fluorescence facility based on polycapillary X-ray optics and Kirkpatrick-Baez mirrors, Spectrochim. Acta B63 (2008) 76–80.
[5] K. Tsuji, K. Nakano, X. Ding, Development of confocal micro X-ray fluorescence instrument using two X-ray beams, Spectrochim. Acta B62 (2007) 549–553.
[6] A. Bjeoumikhov, S. Bjeoumikhova, N. Langhoff, R. Wedell, Polycapillary optics for energy dispersive micro X-ray diffractometry, Appl. Phys. Lett. 86 (144102) (2005) 2005.
[7] T. Sun, Z. Liu, X. Ding, An energy dispersive micro X-ray diffractometer based on a combined system of polycapillary optics, Nucl. Instr. Meth. Phys. Res. B262 (2007) 153–156.
[8] M. Uda, In situ characterization of ancient plaster and pigments on tomb walls in Egypt using energy dispersive X-ray diffraction and fluorescence. Nucl., Instr. Meth. Phys. Res. B B226 (2004) 75–82.
[9] R.D. Perez, H.J. Sánchez, M. Rubio, C.A. Perez, Characterization of home-made x-ray polycapillaries, X-ray Spectrom. 37 (2008) 646–651.
[10] R.D. Perez, M. Rubio, C. Pérez, A. Eynard, G. Bongiovanni, Study of the effects of chronic arsenic poisoning in rat kidneys by means of synchrotron microscopic x-ray fluorescence analysis, X-ray Spectrom. 35 (2006) 352–358.
[11] W. Malzer, B. Kanngießer, A model for the cofocal volume of 3D micro x-ray fluorescence spectrometer, Spectrochim. Acta B60 (2005) 1334–1341.

[12] S.M. Clark, Thirty years of energy-dispersive powder diffraction, Cryst. Rev. 8 (2002) 57–92.
[13] T. Sun, M. Zhang, X. Ding, Z. Liu, X. Lin, H. Liu, Characterization of polycapillary X-ray lens for application in confocal three-dimensional energy dispersive micro X-ray diffraction experiments, J. Appl. Cryst. 40 (2007) 1169–1173.
[14] P. Sarrazin, D. Blake, S. Feldman, S. Chipera, D. Vaniman, D. Bish, Field deployment of a portable XRF/XRD instrument on mars analog terrain, Adv. X-ray Anal. 48 (2005) 194–203.
[15] C. Cardell, I. Guerra, J. Romero-Pastor, G. Cultrone, A. Rodriguez-Navarro, Innovative analytical methodology combining micro-X-ray diffraction, scanning electron microscopy-based mineral maps, and diffuse reflectance infrared Fourier transform spectroscopy to characterize archeological artifacts, Anal. Chem. 81 (2009) 604–611.
[16] K. Geraki, M. Farquharson, D. Bradley, X-ray fluorescence and energy dispersive X-ray diffraction for the characterization of breast tissue, Rad. Phys. Chem. 71 (2004) 969–970.